

# Robustifying Twist-and-Turn Entanglement with Interaction-Based Readout

Safoura S. Mirkhalaf,<sup>1</sup> Samuel P. Nolan,<sup>2</sup> and Simon A. Haine<sup>3</sup>

<sup>1</sup>*QSTAR, Largo Enrico Fermi 2, 50125, Firenze, Italy*

<sup>2</sup>*School of Mathematics and Physics, The University of Queensland, Brisbane, Queensland, Australia*

<sup>3</sup>*Department of Physics and Astronomy, University of Sussex, Brighton, United Kingdom\**

(Dated: December 14, 2024)

The use of multi-particle entangled states has the potential to drastically increase the sensitivity of atom interferometers and atomic clocks. The Twist-and-Turn (TNT) Hamiltonian can create multi-particle entanglement much more rapidly than ubiquitous one-axis twisting (OAT) Hamiltonian in the same spin system. In this paper, we consider the effects of detection noise - a key limitation in current experiments - on the metrological usefulness of these nonclassical states and also consider a variety of interaction-based readouts to maximize their performance. Interestingly, the optimum interaction-based readout is not the obvious case of perfect time reversal.

## I. INTRODUCTION

There is currently considerable interest in methods that can produce highly entangled states of atomic ensembles with the motivation of enhancing the sensitivity of atom interferometers and atomic clocks [1]. Without many-body entanglement, the phase sensitivity of such experiments is fundamentally shot-noise-limited (SNL)  $\Delta\phi = 1/\sqrt{N}$  [2, 3]. In recent years, experiments in atomic systems based on the one-axis twisting (OAT) squeezing scheme of Kitagawa and Ueda [4, 5] have demonstrated metrologically useful spin-squeezing [6, 7], and sub-shot-noise phase detection [8–10]. However, typical experiments are limited to only moderate quantum enhancement due to constraints on the state preparation time imposed by dephasing [11, 12] and multi-mode dynamics [13, 14]. This leads to a degree of quantum enhancement that is considerably less than the theoretical optimum. Recently, a related method known as Twist and Turn (TNT) squeezing has been demonstrated [15–18]. The TNT Hamiltonian, which uses the same nonlinear interactions as OAT with an additional linear rotation, typically reaches larger degrees of quantum enhancement for the same interaction time. As TNT is based on the same interactions that leads to OAT squeezing, it can be implemented in the same experimental set-ups.

In practice, however, it is very difficult to fully exploit the nonclassical features of quantum states. This is mainly due to fragility of quantum correlated states against inevitable sources of noise (e.g. phase or detection noise). Thus, it is very important to look for the theoretical schemes that improve the sensitivity of the precision and yet, are robust against external noises. One way to conquer these effects is to use *interaction-based readout* protocols [19–30] which make use of the appropriate unitary/supplementary operations right before final measurement. These schemes can be summarized as follows: The schemes begin with a state preparation stage, where the quantum Fisher information (QFI) of

the (typically un-entangled) initial state  $|\psi_0\rangle$  is increased via the unitary operator  $U_1$ . The classical parameter to be estimated  $\phi$  is then encoded onto the state via a measurement device (for example, a Mach-Zehnder interferometer) described by the unitary operator  $U_\phi$ . The interaction-based readout is then implemented by applying another unitary operator  $\hat{U}_2$  directly before the final measurement, such that the final state is

$$|\psi\rangle = U_2 U_\phi U_1 |\psi_0\rangle. \quad (1)$$

$U_2$  does not alter the QFI, but *can* effect the classical Fisher information (CFI) when a measurement is made in a particular basis. Specifically, it has been shown that protocols which perfectly time reverse the initial unitary operator ( $U_2 = U_1^\dagger$ , which we refer to as an *echo*) followed by a measurement that projects onto the initial state, saturates the quantum Cramér-Rao bound (QCRB) [22]. It has also been shown that using  $U_2 = U_1^\dagger$  can improve robustness against detection noise [21, 26]. However, in [26] it was shown that when a measurement that resolves the probability of *all* results in a particular basis is made, there are *many* choices of  $U_2$  (including the trivial choice  $U_2 = 1$ ) that saturate the QCRB. Furthermore, in many circumstances, there are choices for  $U_2$  that provide greater robustness than  $U_2 = U_1^\dagger$ . In this paper we investigate how interaction-based readouts improve robustness specifically for the case where the state preparation ( $U_1$ ) and interaction based read-out ( $U_2$ ) are based on the TNT interaction.

## II. INTERACTION-BASED READOUT PROTOCOL

Let us consider an ensemble of  $N$  two-level atoms which are prepared in initial state  $|\psi_0\rangle$ . The interaction-based readout protocol includes the following four steps:

- State preparation** increases the QFI of the initial state via unitary evolution  $U_1$  as  $\rho = U_1 |\psi_0\rangle \langle \psi_0| U_1^\dagger$ . In particular, we use the TNT Hamiltonian for this purpose (next Section).

\* simon.a.haine@gmail.com

ii **Phase encoding.** An unknown phase is encoded into the state by performing linear unitary  $U_\phi = e^{-i\phi\hat{S}_n}$  on the system such that  $U_\phi^\dagger\rho U_\phi$ . This process corresponds to making a rotation around an arbitrary spin direction  $\vec{n}$ .

iii **Interaction-based readout** The second entangling evolution  $U_2$  is applied onto the state as  $U_2U_\phi\rho U_\phi^\dagger U_2^\dagger$ . Echo protocols refer to the special case of perfect time reversal  $U_2 = U_1^\dagger$ . Under certain conditions, which we demonstrate below,  $U_2$  allows measurements made in the appropriate basis to saturate the QCRB.

iv **Spin-resolving measurement.** Here, we make spin-resolving measurements on some complete orthogonal basis  $\{|m\rangle\}$ . This is equivalent to estimating the full probability distribution  $P_m(\phi) = \langle m|U_2U_\phi\rho U_\phi^\dagger U_2^\dagger|m\rangle$ .

Consequently, the phase  $\phi$  can be estimated by examining the probabilities  $P_m(\phi)$ . Based on parameter estimation theory, the precision of the estimate is bounded by  $\Delta\phi^2 = 1/F_c(\phi)$  where

$$F_c(\phi) = \sum_m \frac{1}{P_m(\phi)} \left( \frac{\partial P_m(\phi)}{\partial \phi} \right)^2 \quad (2)$$

is the classical Fisher information (CFI). For single-variate parameter estimation, can be shown [31–33] that a measurement basis yielding  $F_c = F_Q$  is guaranteed to exist. This measurement is optimal - the measurement saturates the ultimate limit of sensitivity, namely, the quantum Crámer-Rao bound. As was shown in [26], the conditions that  $U_2$  and the measurement basis  $\{|m\rangle\}$  saturate the QCRB are (see Appendix A for a more detailed proof):

1. The initial state is the parity eigenstate in the measurement basis  $\{|m\rangle\}$ ; i.e.  $\hat{\Pi}\rho = (-1)^p\rho$  where,  $p = 0, 1$  for  $\hat{\Pi} = \sum_m (-1)^m |m\rangle\langle m|$ .
2. The generator  $\hat{S}_n$  flips the parity; i.e.  $\hat{\Pi}\hat{S}_n\hat{\Pi} = -\hat{S}_n$ .
3. The readout  $U_2$  conserves the parity with respect to the measurement basis,  $[U_2, \hat{\Pi}] = 0$ .

This implies that it is always possible to saturate the QCRB conditioned on suitable choices of measurement basis, readout and phase generator. This conditions (1,2) can be used to determine the optimal measurement basis, which is typically easily accessible. Note that even for the trivial case of readout (ie,  $U_2 = 1$ ), so long as the conditions (1,2) hold the sensitivity saturates the QCRB [34]. Nevertheless, a non-trivial choice of  $U_2$  (ie,  $U_2 \neq 1$ ) often increases the robustness against detection noise. In this spirit, we are allowed to pick the best readout strategy which satisfies the parity conservation requirement (the third condition).

In the following, we consider the TNT Hamiltonian and demonstrate that the conditions for saturating the QCRB are satisfied.

### III. TWIST-AND-TURN INTERFEROMETRY

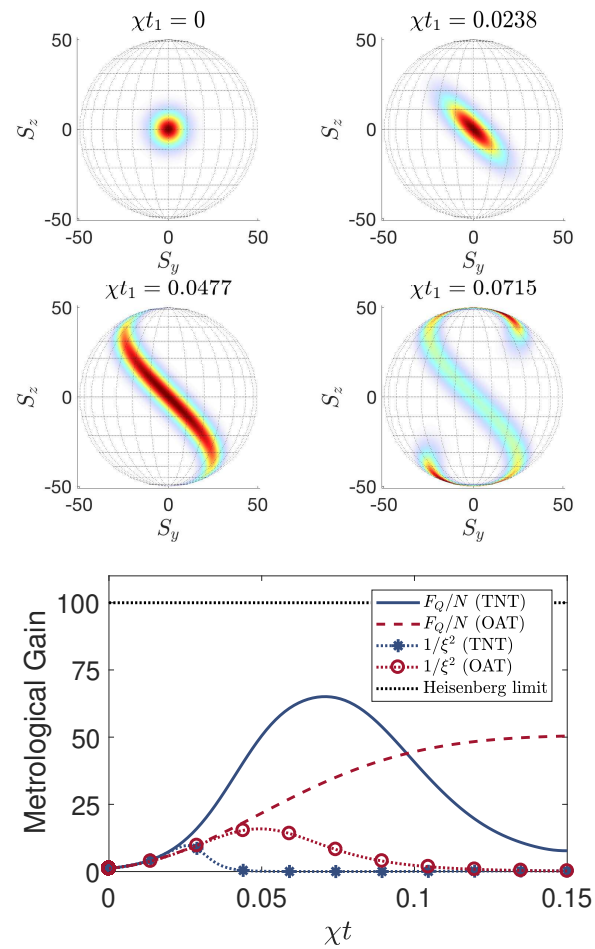


FIG. 1. (Color online) Upper panel: Husimi  $Q$  function for the state  $|\psi\rangle = \exp(-itH_{\text{TNT}})|\psi_0\rangle$  under TNT with  $\Lambda = 2$  and  $N = 100$ , where  $|\psi_0\rangle$  is chosen as the eigenstate of  $\hat{S}_x$  with minimum eigenvalue. From left to right:  $\chi t = 0, 0.0238, 0.0477$ , and  $0.0715$ . The final frame is the time at which the QFI is maximum. Bloch-sphere plots display the  $SU(2)$  Husimi  $Q$ -function  $Q/Q_{\text{max}}$ , which is defined  $Q(\theta, \varphi) = \langle \theta, \varphi | \rho | \theta, \varphi \rangle$ , where  $|\theta, \varphi\rangle = e^{i\varphi\hat{S}_z} e^{i\theta\hat{S}_y} |S_z = N/2\rangle$  represents the spin coherent state along  $\theta$  and  $\varphi$  directions corresponding to rotating the maximal  $\hat{S}_z$  eigenstate around azimuthal and polar angles  $\{\theta, \varphi\}$  [35]. Lower panel: Metrological gain  $F_Q/N$  as a function of  $\chi t$  for TNT (blue solid) and OAT (red dashed). We have also included the gain based on spin-squeezing parameter for TNT (blue solid-pentagram) and OAT (red solid-circled). The Heisenberg limit ( $\Delta\phi = 1/N$ ) is indicated by the black dotted line. The initial state is chosen to be the minimal eigenstate of  $S_x$ .

We consider the TNT Hamiltonian [15–17]

$$H_{\text{TNT}} = \hbar\chi\hat{S}_z^2 - \hbar J\hat{S}_x \quad (3)$$

such that  $U_1 = \exp(-it_1 H_{\text{TNT}}/\hbar)$ , where the adjustable parameter  $t_1$  is the state preparation time. Here, the

collective spin operators obey the usual  $SU(2)$  commutation relations:  $[\hat{S}_i, \hat{S}_j] = \epsilon_{ijk} \hat{S}_k$  where  $\epsilon_{ijk}$  is the Levi-Civita symbol. Moreover,  $\chi$  and  $J$  denote the magnitude of the spin-spin interaction and the rate of rotation about the  $\hat{S}_x$  axis, respectively. One can alter the macroscopic properties of the system by adjusting the parameter  $\Lambda = N\chi/J$  [36, 37], where  $N$  is the total number of particles. Specifically, it has been shown that  $\Lambda = 2$ , corresponding to maximal criticality of the unstable fixed point in mean-field approximation, provides the maximum rate of entanglement generation [15, 18]. In the limit of  $\chi \gg J$  the TNT Hamiltonian reduces into the well-known one-axis-twisting form  $H_{\text{OAT}} = \hbar\chi\hat{S}_z^2$ .

The TNT Hamiltonian can accelerate the rate of entanglement generation compared to the OAT Hamiltonian for the same  $\chi t_1$  [17]. This is the direct consequence of interplay between twist ( $\propto \hat{S}_z^2$ ) and turn ( $\propto \hat{S}_x$ ) terms of the Hamiltonian. The generation of spin-squeezing under TNT dynamics has been investigated theoretically [15–18, 38] and realized experimentally in systems of Bose-Einstein Condensation [16, 17] and atomic ensembles [39].

Figure (1) shows the time evolution of the  $SU(2)$  Husimi  $Q$ -function [35, 40], and the QFI under TNT dynamics. The QFI is defined as  $F_Q = 4\Delta S_n^2$ , where  $\hat{S}_n$  is the collective spin operator pointing in the direction that maximises the QFI [41]. However, the QFI is silent on what measurement choice saturates the QCRB. If the  $\phi$  estimate is obtained from the mean spin component  $\langle \hat{S}_{n'} \rangle$ , the error propagation formula gives  $\Delta\phi^2 = \Delta S_{n'}^2 / \partial_\phi \langle \hat{S}_{n'} \rangle = \xi^2 / N$ , where  $\xi^2 = N\Delta S_{n'}^2 / \langle \hat{S}_{\parallel} \rangle^2$  is the spin-squeezing parameter normal to mean spin direction  $\hat{S}_{\parallel}$  [42]. For small values of  $\chi t$ , this method of estimation is very close to the QCRB, but breaks down as the state becomes non-Gaussian. These states are called entangled non-Gaussian states (ENGs). An analysis of their CFI reveals they can outperform the metrological gain accessible with spin-squeezed states [3, 16, 21, 22, 43].

We now consider the requirements for performing a measurement that saturates the QCRB with a state generated via TNT dynamics. Assuming that the initial state is an eigenstate of  $\hat{S}_x$ , then  $H_{\text{TNT}}$  couples only to  $\hat{S}_x$  eigenstates of the same parity. That is,  $U_1$  conserves parity with respect to the  $\hat{S}_x$  basis  $\{|m\rangle_x\}$  [44, 45]. Subsequently, we align the interferometer along the optimal  $F_Q$  direction such that  $U_\phi = \exp(i\hat{S}_n\phi)$ . It has been shown that this operator is in the  $y-z$  plane, ie,  $\hat{S}_n = \alpha\hat{S}_y + \beta\hat{S}_z$  normal to the mean spin direction  $\hat{S}_x$  [18]. Since the generator of the interferometer  $\hat{S}_n$  flips the parity (ie,  $\hat{\Pi}\hat{S}_n\hat{\Pi} = -\hat{S}_n$ , for  $\hat{\Pi} = \sum_m |m\rangle_x \langle m|_x$ ), we see that a measurement that projects into the  $\hat{S}_x$  basis will saturate the QCRB. This is applicable for all the readouts that conserves parity with respect to  $\hat{S}_x$  (see Appendix B for details).

In realistic situation however, there is detection noise which affects the estimation sensitivity. This is a key limitation in current experiments. Both spin-squeezed

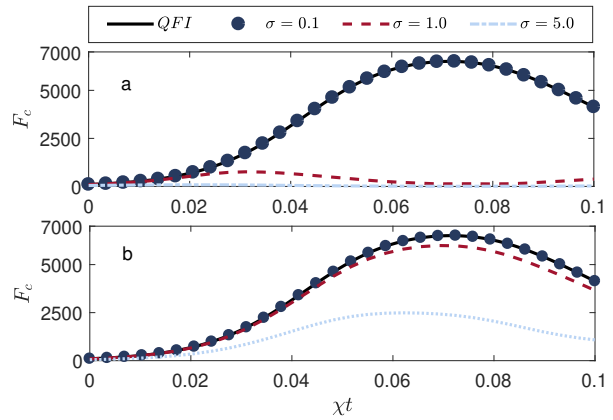


FIG. 2. (Color online) Time evolution of the QFI (solid black) and CFI for various detection noises  $\sigma = 0.1$  (dotted blue), 1 (dashed red) and 5 (dotted-dashed light turquoise) for the final state  $U_2 U_\phi U_1 |\psi_0\rangle$ , for (a):  $U_2 = 1$ , and (b):  $U_2 = U_1^\dagger$ . In all cases the initial state is chosen to be the minimal eigenstate of  $S_x$  and we have fixed  $\phi = 10^{-4}$ .

states and ENGs are more sensitive to detection noise than un-entangled states of the same size, and ENGs typically demand detection noise at the single-atom level [1, 25, 46], which restricts them to small numbers as the requisite counting efficiency rapidly becomes impossible.

The effect of detection noise is to introduce additional, classical noise to the measurement process. For example, a detector that measures the spin projection along  $\hat{S}_x$  should always read  $S_x = N/2$  for a maximal  $\hat{S}_x$  eigenstate. However, if there is noise introduced, there is a finite chance that the detector will read  $S_x = m \neq N/2$ . To model detection noise we take the convolution of the probability distribution with a Gaussian distribution [47] with detection noise  $\sigma$ ,

$$\tilde{P}_m(\phi) = \sum_{m'} C_{m'}(\sigma) e^{-(m-m')^2/2\sigma^2} P_{m'}(\phi) \quad (4)$$

where  $C_{m'}(\sigma)$  is normalization factor such that

$$\sum_{m'} C_{m'} e^{-(m-m')^2/2\sigma^2} = 1. \quad (5)$$

In Figure (2a) we show the CFI calculated from this convolved probability distribution  $\tilde{P}_m$  for the state  $U_\phi U_1 |\psi_0\rangle$ , for different values of  $\sigma$ . For  $\sigma \lesssim 0.1$ , our measurement saturates the QCRB. However, for moderate values of  $\chi t_1$ , a small increase in detection noise significantly degrades the sensitivity. However, by adding an interaction-based readout such that the final state is (Figure (2b))  $U_2 U_\phi U_1 |\psi_0\rangle$ , with  $U_2 = U_1^\dagger$ , the sensitivity is much more robust to the presence of noise.

We can understand why the interaction-based echo makes the system so much more robust by looking at

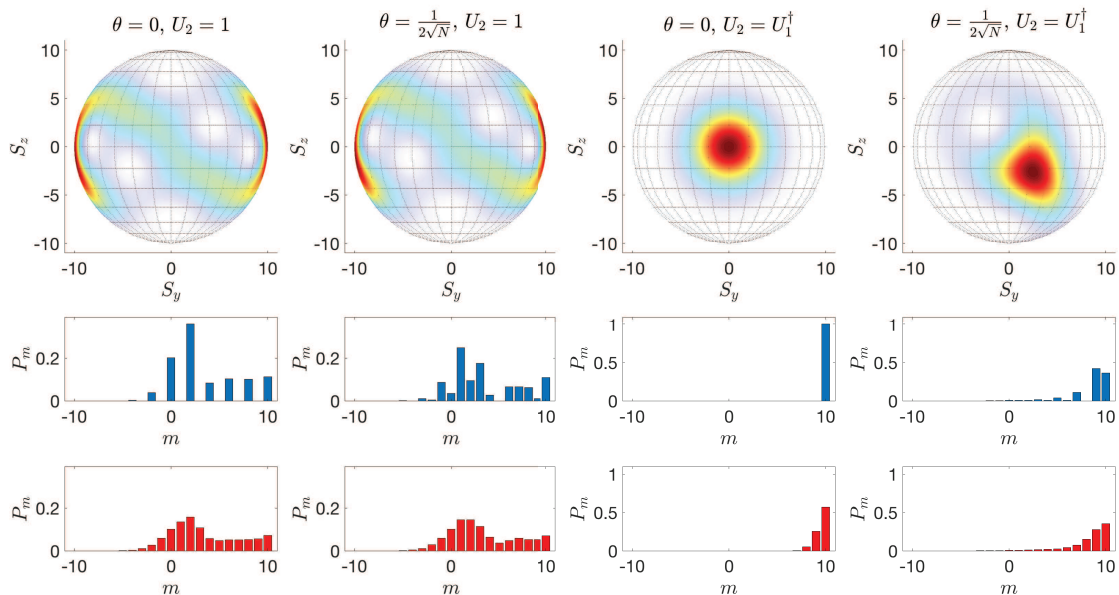


FIG. 3. (Color online) Top row: Husimi  $Q$  function for the final state for (from left to right):  $\phi = 0, U_2 = 1$ ;  $\phi = \frac{1}{2\sqrt{N}}, U_2 = 1$ ;  $\phi = 0, U_2 = U_1^\dagger$ ;  $\phi = \frac{1}{\sqrt{N}}, U_2 = U_1^\dagger$ . Middle row (blue histograms): The corresponding probabilities  $P_m$  for measurements in the  $S_x$  basis for these same states. Bottom row (red histograms): Probabilities in the  $S_x$  basis convolved with detection noise with  $\sigma = 1$ . Parameters:  $N = 20$ ,  $\Lambda = 2$  and  $\chi t = 0.275$ , which is maximises  $F_Q$ . Note that for reasons of visual clarity, we have rotated the state around the  $S_x$  axis such that  $S_n = S_y$ .

the  $Q$ -function and the probability distributions. Figure (3) shows the  $Q$ -functions and  $S_x$  probability distribution for states with  $\phi = 0$  and a small phase shift  $\delta\phi$ , for the case with ( $U_2 = U_1^\dagger$ ) and without ( $U_2 = 1$ ) an interaction-based readout. Specifically, in this example we choose  $U_2 = U_1^\dagger$ . Of course, the fidelity between the state  $\phi = 0$  and  $\delta\phi$  is identical with and without the interaction-based readout. Similarly, the Hellinger distance between the distributions is also identical. The Hellinger distance is defines a statistical distance between  $P_m(\phi_1)$  and  $P_m(\phi_2)$ , defined as  $d_h^2(\phi_1, \phi_2) = 1 - \sum_m \sqrt{P_m(\phi_1)P_m(\phi_2)}$ . Adding detection noise, it becomes difficult to distinguish the distributions when  $U_2 = 1$ . Compare this to  $U_2 = U_1^\dagger$ , and the two distributions are more easily distinguished. Quantitatively, without the interaction-based readout, the Hellinger distance is  $d_h^2 = 0.01$ , but when we include the readout it is significantly larger:  $d_h^2 = 0.17$  (compared to  $d_h^2 = 0.40$  in both cases when no noise is included). However, there is no guarantee that  $U_2 = U_1^\dagger$  is the best choice of interaction-based readout. In the next section, we examine several possibilities to determine what is the best choice for maximising robustness in TNT squeezing.

#### IV. ROBUSTIFYING ENTANGLEMENT AGAINST DETECTION NOISE

We now examine the robustness to detection noise, for a different choices of  $U_2$ , all satisfying the conditions for optimality. In particular, we chose the trivial case of no interaction-based readout ( $U_2 = 1$ ), and the simple time-reversal read-out ( $U_2 = U_1^\dagger(t_2)$ ). The latter choice includes asymmetric echo where  $t_2 \neq t_1$ , which implies  $U_2 \neq U_1^\dagger$ . In this case, we have increased the interaction time for the read-out compared to the state preparation step. Moreover, We also include  $U_2 = U_1$ , which may be applicable in the case when it is not easy to reverse the sign of the interaction constant  $\chi$ , such as when one is working with bright-solitons [48], or enhanced nonlinear interactions due to state-dependent potentials [9].

Figure 4 shows  $F_c$  as a function of detection noise for different choices of  $U_2$  when  $\chi t_1 = 0.027$  (when the metrological gain using the spin squeezing parameter is maximum) and  $0.072$  (when the QFI is maximum). For the case of weak entanglement ( $\chi t_1 = 0.027$ ), we see that the trivial case ( $U_2 = 1$ ) is degraded to below shot-noise levels for noise of approximately  $\sigma \approx 4.40$ . However, by adding the ‘echo’ unitary ( $U_2 = U_1^\dagger$ ), sub-shot-noise sensitivities are retained up to  $\sigma \approx 16.45$ . Interestingly the choice  $U_2 \neq U_1^\dagger$  provides greater robustness again, with sub-shot-noise sensitivities with up to  $\sigma = 39.17$ ,

which is significantly greater than  $\sqrt{N}$ . For this value of  $\chi t_1$ ,  $U_2 = U_1$  provides no advantage compared to the trivial case. However, for the case of maximum QFI ( $\chi t = 0.072$ ), this choice does provide some additional robustness compared to the trivial case. The asymmetric echo provides the greatest robustness of the schemes considered, and therefore may be useful when there is unavoidably large detection noise. To obtain  $F_c$ , we have numerically optimised the measurement basis in the planes normal to  $\hat{S}_x$  and  $\hat{S}_n$  [49]. Based on our numerical calculations, it seems that by increasing the detection noise, the optimal measurement basis moves into the normal plane to  $S_x$ .

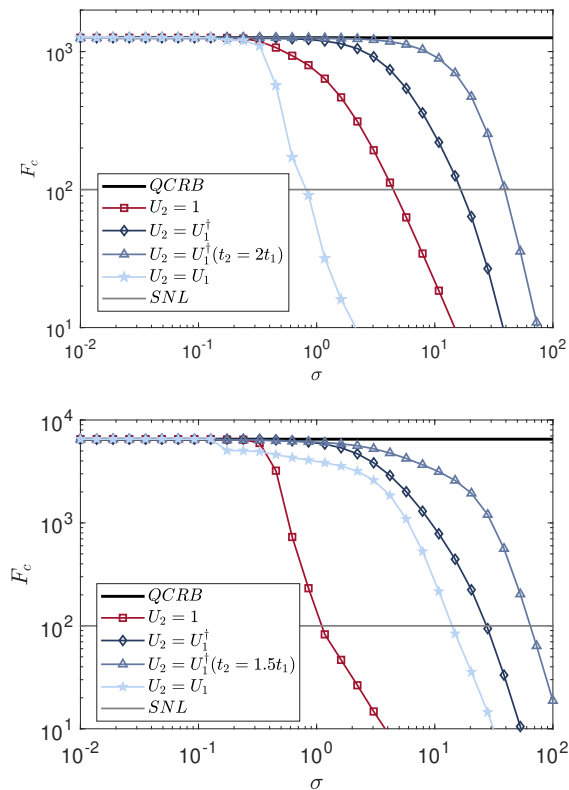


FIG. 4. (Color online) Decay of classical Fisher information a many-body entangled state produced by TNT Hamiltonian in presence of detection noise  $\sigma$  for  $N = 100$ ,  $\Lambda = 2$  and  $\chi t_1 = 0.027$  (upper panel) and  $\chi t_1 = 0.072$  (lower panel). We have considered the trivial protocol  $U_2 = 1$  (red squares), an echo  $U_2 = U_1^\dagger$  (dark blue diamonds), an asymmetric echo  $U_2 \neq U_1^\dagger$  (light blue triangles) and a pseudo-echo  $U_2 = U_1$  (light turquoise pentagrams). We have also considered QCRB and SNL as thick black and thin grey lines respectively. Here,  $\phi = 10^{-4}$ .

We now more closely examine the effect of an asymmetric echo on the TNT scheme. In figure 5, we have changed the time duration of the echo  $t_2/t_1$  for fixed detection noises  $\sigma = 0.1, 5.0$  when the TNT Hamiltonian produces the maximum value of spin squeezing ( $t_1 = 0.027$ ) or maximum value of quantum Fisher in-

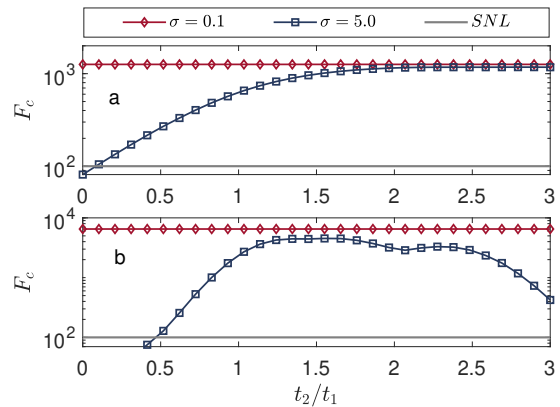


FIG. 5. (Color online) The Fisher information produced by TNT versus time duration of echo  $t_2/t_1$  for  $U_2 = U_1^\dagger(t_2)$  in presence of detection noise  $\sigma = 0.1$  (red diamonds) and 5 (blue squares) when (a): spin squeezing is maximum  $t_1 = 0.027$  and (b): when quantum Fisher information is maximum  $t_1 = 0.072$ . For both cases, when there is negligible detection noise, the extracted Fisher information corresponds to QCRB as expected. The SNL is represented by dashed grey line.

formation ( $t_1 = 0.072$ ) respectively. For small values of detection noise  $\sigma = 0.1$ ,  $U_2$  does not affect the classical Fisher information. In this case, as mentioned before,  $F_c$  saturates the QCRB. In contrast, for more noise ( $\sigma = 5.0$ ) we see that in the Gaussian regime ( $t_1 = 0.027$ ), by increasing the duration of the echo ( $t_2/t_1$ ) the sensitivity becomes more robust against detection noise and eventually approaches the QCRB value for large enough duration of echo. On the other hand, in the non-Gaussian entangled regime ( $t_1 = 0.072$ ), the robustness of  $F_c$  increases by growing the time of echo up to around 1.5 and then it decrease again. Very recently, the similar behaviour has been reported in two-axis-counter-twisted interaction-based readout scheme [28].

In a realistic spin-squeezing set-up, the duration of the experiment may be limited by the particle losses as well as dephasing [11, 12] and multi-mode dynamics [13, 14]. Therefore, it is important to consider the optimal portion of time for entangling ( $U_1$ ) and re-entangling ( $U_2$ ) sequences, as there is a trade-off between the desire to maximise the QFI via the state preparation operation  $U_1(t_1)$ , and robustifying against detection noise via the interaction-based readout operation  $U_2(t_2)$ , while keeping the total time fixed  $T = t_1 + t_2$ . In Figure 6 we have given the optimized Fisher information versus entangling unitary time for total experimental duration  $T = 0.1$  with  $N = 100$  and  $\Lambda = 2$  and time reversal echo case  $U_2 = U_1^\dagger$ . When the detection noise is small ( $\sigma = 0.1$ ), there is little benefit in increasing  $t_2$  and the optimum strategy is to choose  $U_2 = 1$ . However this is certainly not true for large detection noise, as devoting more time to the entangling operation compromises the interaction-based readout. Therefore, there is a balance to be found between increasing the CFI via increasing  $t_1$  and Robustifying the

state via increased  $t_2$ . For larger values of detection noise ( $\sigma = 1.0, 5.0$ ) we see that the optimal strategy is close to an echo ( $t_1 \approx T/2 = 0.050$ ). The reason is that when we devote less than half of the time to the TNT entangling operation, there is always a possibility to perform an echo with  $t_2/t_1 \geq 1$ . Thus, the decrease in  $F_c$  as a result of reducing the first TNT unitary is compensated for by increased robustness provided by the second unitary. For instance Figure 5a gives the typical behaviour of the asymmetric echo within this region, which approaches to the QCRB as  $t_2/t_1$  increases beyond 1. On the other hand, by increasing the portion of the entangling duration more than  $T/2$ , the echo time ratio  $t_2/t_1$  decreases less than unity, and is far more susceptible to detection noise.

## V. CONCLUSION

Many-body entangled states are a crucial resources for quantum-enhanced metrology. Current experiments are working to devise schemes that are able to rapidly manufacture these states in large atomic ensembles, but currently detection noise is a key limitation [1]. The TNT interaction is capable of generating entanglement faster than the conventional one-axis-twisting interaction. TNT is capable of rapidly producing both spin-squeezed states and ENGS. In this work we explore the use of interaction-based readout protocols to provide rapid quantum-enhanced metrology based on twist-and-turn dynamics, which is also robust to detection noise and optimally utilises the state's entanglement. This is done with a spin-resolving measurement in the optimal basis, which we provide criteria for determining. In this regard, we have confirmed the usefulness of standard symmetric echo protocols in boosting the measurement performance against noise. However, our results imply that for weak initial entangling, using an asymmetric echo provides better robustness than the former case. Finally, we have considered TNT echo protocols in realistic situation where there is a limitation on the total time allowed for both the initial interaction and the readout. We have shown that the best outcomes requires the balance between entangling and re-entangling time durations. When the noise is small, any readout is sub-optimal. In presence of considerable noise, the optimal strategy is close to an echo, but the precise time trade-off depends on the noise present in the system.

## VI. ACKNOWLEDGEMENTS

The authors acknowledge useful discussions with Augusto Smerzi, Luca Pezze, and Manuel Gessner. Numerical simulations were performed on the University of Queensland School of Mathematics and Physics computing cluster ‘‘Dogmatix,’’ with thanks to I. Mortimer for computing support. S.P.N. acknowledges support pro-

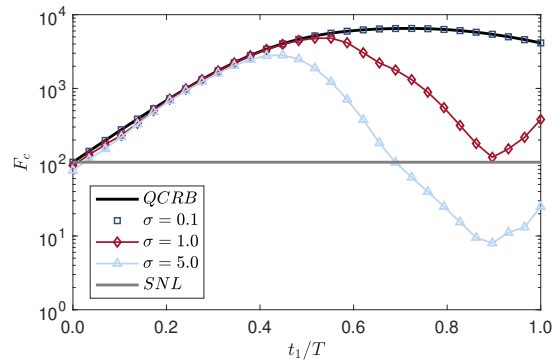


FIG. 6. (Color online) Classical Fisher information versus entangling duration  $t_1$ , with fixed total experimental time  $\chi T = \chi(t_1 + t_2) = 0.1$ . The TNT entanglement and re-entangling operation ( $U_2 = U_1^\dagger(t_2)$ ) are applied for durations  $t_1$  and  $t_2 = T - t_1$  respectively, such that  $|\psi_\phi\rangle = U_1^\dagger(t_2)U_\phi U_1(t_1)|\psi_0\rangle$ . Here,  $N = 100$  and  $\Lambda = 2$  and we have considered  $\sigma = 0.1$  (dark blue squares),  $1.0$  (red diamonds) and  $\sigma = 5.0$  (light turquoise triangles). The QCRB and SNL are given with solid thick black and thin grey lines.

vided by an Australian Postgraduate Award. S.A.H. has received funding from the European Union’s Horizon 2020 research and innovation programme under the Marie Skłodowska-Curie Grant Agreement No. 704672.

## Appendix A: The conditions of QCRB saturation

Here, we present our conditions for saturation of QCRB (Section 2) when applying spin-resolving measurement [26].

To begin, let’s ignore the re-entangling readout operator, and consider only  $U_2 = 1$ . After the state preparation and phase encoding steps, the probability of estimating the small, unknown phase  $\phi$  is given by  $P_m(\phi) = \langle m|U_\phi \rho U_\phi^\dagger|m\rangle$  with  $U_\phi = e^{(-iS_n\phi)}$ . Our phase estimation is limited by the CFI. For small values of  $\phi$  the CFI can be approximated as the leading term in the expansion of the Hellinger statistical distance in the space of probability distributions[16]

$$\begin{aligned} d_H^2(0, \phi) &= 1 - \sum_m \sqrt{P_m(0)P_m(\phi)} \\ &= F_c(0)\phi^2/8 + \mathcal{O}(\phi^3) \end{aligned} \quad (\text{A1})$$

For small  $\phi$ , Taylor expanding the probability amplitude gives

$$\begin{aligned} P_m(\phi) &= P_m(0) + \left. \frac{\partial P_m(\phi)}{\partial \phi} \right|_{\phi=0} \phi + \left. \frac{\partial^2 P_m(\phi)}{\partial \phi^2} \right|_{\phi=0} \frac{\phi^2}{2} \\ &+ \mathcal{O}(\phi^3). \end{aligned} \quad (\text{A2})$$

We have

$$\begin{aligned}
P_m(\phi) &= \langle m|U_\phi^\dagger \rho U_\phi|m\rangle, \\
\frac{\partial P_m(\phi)}{\partial \phi} &= i\langle m|\hat{S}_n U_\phi \rho U_\phi^\dagger|m\rangle + c.c. \\
\frac{\partial^2 P_m(\phi)}{\partial \phi^2} &= \langle m|\hat{S}_n U_\phi \rho U_\phi^\dagger \hat{S}_n|m\rangle \\
&\quad - \langle m|\hat{S}_n^2 U_\phi \rho U_\phi^\dagger|m\rangle + c.c. \quad (A3)
\end{aligned}$$

which leads to

$$\begin{aligned}
P_m(0) &= \langle m|\rho|m\rangle, \\
\left. \frac{\partial P_m(\phi)}{\partial \phi} \right|_{\phi=0} &= i\langle m|\hat{S}_n \rho|m\rangle + c.c. \\
\left. \frac{\partial^2 P_m(\phi)}{\partial \phi^2} \right|_{\phi=0} &= \langle m|\hat{S}_n \rho \hat{S}_n|m\rangle \\
&\quad - \langle m|\hat{S}_n^2 \rho|m\rangle + c.c. \quad (A4)
\end{aligned}$$

Now, suppose that the density operator is an eigenstate of parity operator  $\hat{\Pi} = \sum_m (-1)^m |m\rangle\langle m|$  such that  $\hat{\Pi}\rho = (-1)^p \rho$  for  $p = 0, 1$ . Also, let  $\hat{\Pi}\hat{S}_n\hat{\Pi} = -\hat{S}_n$  (Section II). Under these two conditions,

$$\begin{aligned}
\langle m|\rho|m\rangle &= (-1)^{m+p} \langle m|\rho|m\rangle, \\
\langle m|\rho \hat{S}_n|m\rangle &= 0, \\
\langle m|\hat{S}_n \rho \hat{S}_n|m\rangle &= (-1)^{m+p+1} \langle m|\hat{S}_n \rho \hat{S}_n|m\rangle, \quad (A5)
\end{aligned}$$

which also yields

$$P_m(0) \langle m|\hat{S}_n \rho \hat{S}_n|m\rangle = 0, \quad (A6)$$

as  $P_m(0) = 0$  if  $m + p$  is odd, and  $\langle m|\hat{S}_n \rho \hat{S}_n|m\rangle = 0$  if  $m + p$  is even. After using A2 and A6 in A1 following by a binomial expansion of square root for small  $\phi$ , we obtain

$$d_H^2(\phi) = \sum_m \langle m|\hat{S}_n^2 \rho|m\rangle / 2 \quad (A7)$$

up to third order in  $\phi$ . Consequently, considering A5, the Fisher information is

$$\begin{aligned}
F_c(0) &= 4 \sum_m \langle m|\hat{S}_n^2 \rho|m\rangle \\
&= 4\Delta \hat{S}_n^2 \\
&= F_Q \quad (A8)
\end{aligned}$$

where,  $\Delta \hat{S}_n^2$  is the variance of generator. The last equality appears since  $F_c \leq F_Q \leq \Delta \hat{S}_n^2$ . This means that the QCRB is satisfied under the two first parity conditions (section II)[50]. As we see, there is no need to use the re-entangling step to obtain the optimal bound of estimation. However, In order to robustify the scheme against noise, we include the readout operator  $U_2$  after phase encoding which gives,  $P_m(\phi) = \langle m|U_2^\dagger U_\phi^\dagger \rho U_\phi U_2|m\rangle$ . This probability function is equal to  $\langle m|U_\phi^\dagger \rho U_\phi|m\rangle$  if  $[U_2, \hat{\Pi}] = 0$ , i.e. the readout operator has the same parity parity as measurement basis  $|m\rangle$  (condition 3 given in section II).

### Appendix B: Fulfilment of parity conditions for TNT scenario

The TNT Hamiltonian spectrum has a fixed parity of the projection  $\hat{S}_x$  due to  $[H_{\text{TNT}}, \hat{\Pi}_x] = 0$  [44, 45]. The symmetries of the Hamiltonian imply that the dynamics is restricted to the odd and even eigenstates of  $\hat{S}_x$ . Consequently by taking the initial state as  $\hat{S}_x$  eigenstate, the first parity condition of section II is satisfied. Moreover, the parity symmetry leads to  $\hat{\Pi}_x(\hat{S}_x, \hat{S}_y, \hat{S}_z)\hat{\Pi}_x = (\hat{S}_x, -\hat{S}_y, -\hat{S}_z)$ . Considering the fact that optimal QFI is in the  $y - z$  plane [16, 18]  $\hat{S}_n = \alpha \hat{S}_y + \beta \hat{S}_z$ , one obtains  $\hat{\Pi}_x \hat{S}_n \hat{\Pi}_x = -\hat{S}_n$  which demonstrates the second condition. To demonstrate the third condition, we again note that the re-entangling unitary acting on the  $\hat{S}_x$  basis states preserves parity, such that they remain parity eigenstates. Of course, the asymmetry of the time evolution still preserves the parity.

- 
- [1] L. Pezze, A. Smerzi, M. K. Oberthaler, R. Schmied, and P. Treutlein, "Quantum metrology with nonclassical states of atomic ensembles," arXiv:1609.01609 (2016).
- [2] Vittorio Giovannetti, Seth Lloyd, and Lorenzo Maccone, "Quantum metrology," Phys. Rev. Lett. **96**, 010401 (2006).
- [3] Luca Pezzé and Augusto Smerzi, "Entanglement, nonlinear dynamics, and the Heisenberg limit," Phys. Rev. Lett. **102**, 100401 (2009).
- [4] Masahiro Kitagawa and Masahito Ueda, "Squeezed spin states," Phys. Rev. A **47**, 5138–5143 (1993).
- [5] Klaus Mølmer and Anders Sørensen, "Multi-particle entanglement of hot trapped ions," Phys. Rev. Lett. **82**, 1835–1838 (1999).
- [6] J. Esteve, C. Gross, Weller. A., S. Giovanazzi, and M. K. Oberthaler, "Squeezing and entanglement in a Bose-Einstein condensate," Nature **455**, 1216 (2008).
- [7] Ian D. Leroux, Monika H. Schleier-Smith, and Vladan Vuletić, "Implementation of cavity squeezing of a collective atomic spin," Phys. Rev. Lett. **104**, 073602 (2010).
- [8] C. Gross, T. Zibold, E. Nicklas, J. Estève, and M. K. Oberthaler, "Nonlinear atom interferometer surpasses classical precision limit," Nature **464**, 1165–1169 (2010).
- [9] Max F. Riedel, Pascal Böhi, Yun Li, Theodor W. Hänsch, Alice Sinatra, and Philipp Treutlein, "Atom-chip-based generation of entanglement for quantum metrology," Nature **464**, 1170–1173 (2010).
- [10] W. Muessel, H. Strobel, D. Linnemann, D. B. Hume, and M. K. Oberthaler, "Scalable spin squeezing for quantum-enhanced magnetometry with bose-einstein condensates," Phys. Rev. Lett. **113**, 103004 (2014).

- [11] Yun Li, Y. Castin, and A. Sinatra, “Optimum spin squeezing in bose-einstein condensates with particle losses,” *Phys. Rev. Lett.* **100**, 210401 (2008).
- [12] Yun Li, P. Treutlein, J. Reichel, and A. Sinatra, “Spin squeezing in a bimodal condensate: spatial dynamics and particle losses,” *The European Physical Journal B* **68**, 365–381 (2009).
- [13] Simon A. Haine and Mattias T. Johnsson, “Dynamic scheme for generating number squeezing in Bose-Einstein condensates through nonlinear interactions,” *Phys. Rev. A* **80**, 023611 (2009).
- [14] S. A. Haine, J. Lau, R. P. Anderson, and M. T. Johnsson, “Self-induced spatial dynamics to enhance spin squeezing via one-axis twisting in a two-component Bose-Einstein condensate,” *Phys. Rev. A* **90**, 023613 (2014).
- [15] A. Micheli, D. Jaksch, J. I. Cirac, and P. Zoller, “Many-particle entanglement in two-component bose-einstein condensates,” *Phys. Rev. A* **67**, 013607 (2003).
- [16] H. Strobel, W. Muessel, D. Linnemann, T. Zibold, D. B. Hume, L. Pezzè, A. Smerzi, and M. K. Oberthaler, “Fisher information and entanglement of non-gaussian spin states,” *Science* **345**, 424–427 (2014).
- [17] W. Muessel, H. Strobel, D. Linnemann, T. Zibold, B. Juliá-Díaz, and M. K. Oberthaler, “Twist-and-turn spin squeezing in bose-einstein condensates,” *Phys. Rev. A* **92**, 023603 (2015).
- [18] G. Sorelli, L. Pezze, and A. Smerzi, “Fast generation of entanglement in bosonic josephson junctions,” arXiv:1511.01835 (2015).
- [19] A. M. Marino, N. V. Corzo Trejo, and P. D. Lett, “Effect of losses on the performance of an su(1,1) interferometer,” *Phys. Rev. A* **86**, 023844 (2012).
- [20] O. Hosten, R. Krishnakumar, N. J. Engelsen, and M. A. Kasevich, “Quantum phase magnification,” *Science* **352**, 1552–1555 (2016).
- [21] E. Davis, G. Bentsen, and M. Schleier-Smith, “Approaching the heisenberg limit without single-particle detection,” *Phys. Rev. Lett.* **116**, 053601 (2016).
- [22] Tommaso Macrì, Augusto Smerzi, and Luca Pezzè, “Loschmidt echo for quantum metrology,” *Phys. Rev. A* **94**, 010102 (2016).
- [23] Florian Fröwis, Pavel Sekatski, and Wolfgang Dür, “Detecting large quantum fisher information with finite measurement precision,” *Phys. Rev. Lett.* **116**, 090801 (2016).
- [24] Stuart S. Szigeti, Robert J. Lewis-Swan, and Simon A. Haine, “Pumped-up su(1,1) interferometry,” *Phys. Rev. Lett.* **118**, 150401 (2017).
- [25] Emily Davis, Gregory Bentsen, Tracy Li, and Monika Schleier-Smith, “Advantages of interaction-based readout for quantum sensing,” (2017) pp. 101180Z–101180Z–10.
- [26] Samuel P. Nolan, Stuart S. Szigeti, and Simon A. Haine, “Optimal and robust quantum metrology using interaction-based readouts,” *Phys. Rev. Lett.* **119**, 193601 (2017).
- [27] Jiahao Huang, Min Zhuang, and Chaohong Lee, “Non-gaussian precision metrology via driving through quantum phase transitions,” *Phys. Rev. A* **97**, 032116 (2018).
- [28] F. Anders, L. Pezze, A. Smerzi, and C. Klempt, “Phase magnification by two-axis counter-twisting for detection noise robust interferometry.” arXiv:1711.02658 (2017).
- [29] R. Fang, R. Sarkar, and S. M. Shahriar, “Enhancing sensitivity of an atom interferometer to the heisenberg limit using increased quantum noise,” arXiv:1707.08260 (2017).
- [30] A. J. Hayes, S. Dooley, W. J. Munro, K. Nemoto, and J. Dunningham, “Making the most of time in quantum metrology: concurrent state preparation and sensing,” arXiv:1801.03452 (2018).
- [31] Samuel L. Braunstein and Carlton M. Caves, “Statistical distance and the geometry of quantum states,” *Phys. Rev. Lett.* **72**, 3439–3443 (1994).
- [32] Géza Tóth and Iagoba Apellaniz, “Quantum metrology from a quantum information science perspective,” *Journal of Physics A: Mathematical and Theoretical* **47**, 424006 (2014).
- [33] Rafał Demkowicz-Dobrzański, M. Jarzyna, and J. Kołodyński, “Quantum limits in optical interferometry,” *Progress in Optics* **345** (2015).
- [34] Also, note that using  $U_2$  does not change the QFI. This can be easily verified when using the equation  $F_Q = 4[|\langle \partial_\phi \psi | \partial_\phi \psi \rangle - |\langle \psi | \partial_\phi \psi \rangle|^2]$  for  $|\psi\rangle = U_2 U_\phi U_1 |\psi_0\rangle$  where  $\partial_\phi = \partial / \partial \phi$ .
- [35] F. T. Arecchi, Eric Courtens, Robert Gilmore, and Harry Thomas, “Atomic coherent states in quantum optics,” *Phys. Rev. A* **6**, 2211–2237 (1972).
- [36] A. Smerzi, S. Fantoni, S. Giovanazzi, and S. R. Shenoy, “Quantum coherent atomic tunneling between two trapped bose-einstein condensates,” *Phys. Rev. Lett.* **79**, 4950–4953 (1997).
- [37] G. J. Milburn, J. Corney, E. M. Wright, and D. F. Walls, “Quantum dynamics of an atomic bose-einstein condensate in a double-well potential,” *Phys. Rev. A* **55**, 4318–4324 (1997).
- [38] Guang-Ri Jin and Sang Wook Kim, “Spin squeezing and maximal-squeezing time,” *Phys. Rev. A* **76**, 043621 (2007).
- [39] Souma Chaudhury, Seth Merkel, Tobias Herr, Andrew Silberfarb, Ivan H. Deutsch, and Poul S. Jessen, “Quantum control of the hyperfine spin of a cs atom ensemble,” *Phys. Rev. Lett.* **99**, 163002 (2007).
- [40] G. S. Agarwal, “State reconstruction for a collection of two-level systems,” *Phys. Rev. A* **57**, 671–673 (1998).
- [41] Philipp Hyllus, Otfried Gühne, and Augusto Smerzi, “Not all pure entangled states are useful for sub-shot-noise interferometry,” *Phys. Rev. A* **82**, 012337 (2010).
- [42] D. J. Wineland, J. J. Bollinger, W. M. Itano, F. L. Moore, and D. J. Heinzen, “Spin squeezing and reduced quantum noise in spectroscopy,” *Phys. Rev. A* **46**, R6797–R6800 (1992).
- [43] Simon A. Haine and Stuart S. Szigeti, “Quantum metrology with mixed states: When recovering lost information is better than never losing it,” *Phys. Rev. A* **92**, 032317 (2015).
- [44] Pedro Ribeiro, Julien Vidal, and Rémy Mosseri, “Thermodynamical limit of the lipkin-meshkov-glick model,” *Phys. Rev. Lett.* **99**, 050402 (2007).
- [45] Tommaso Caneva, Tommaso Calarco, and Simone Montangero, “Entanglement-storage units,” *New Journal of Physics* **14**, 093041 (2012).
- [46] Samuel P. Nolan and Simon A. Haine, “Quantum fisher information as a predictor of decoherence in the preparation of spin-cat states for quantum metrology,” *Phys. Rev. A* **95**, 043642 (2017).
- [47] Luca Pezzè and Augusto Smerzi, “Ultrasensitive two-mode interferometry with single-mode number squeezing,” *Phys. Rev. Lett.* **110**, 163604 (2013).

- [48] S. A. Haine, “Quantum noise in bright soliton matter-wave interferometry,” *New Journal of Physics* (2018).
- [49] In order to numerically evaluate the optimal value of the CFI in the presence of detection noise, we have considered the optimization of the measurement basis in the planes normal to  $\hat{S}_n$  as well as  $\hat{S}_x$ .
- [50] Note that though the nominator of 2 gives  $\partial_\phi = 0$  for all  $m$ 's, the denominator also gives zero due to parity condition A5. As a result, Fisher information has generally a nonzero value.